BJR

Received: 1 February 2016 | Revised: 9 April 2016 | Accepted: 18 April 2016

http://dx.doi.org/10.1259/bjr.20160115

Cite this article as:
Bulakbasi N, Cancuri O, Kocaoğlu M. The middle interhemispheric variant of holoprosencephaly: magnetic resonance and diffusion tensor imaging findings. *Br J Radiol* 2016; **89**: 20160115.

FULL PAPER

The middle interhemispheric variant of holoprosencephaly: magnetic resonance and diffusion tensor imaging findings

NAIL BULAKBASI, MD, OSMAN CANCURI, MD and MURAT KOCAOĞLU, MD

Department of Radiology, Faculty of Medicine, Near East University, Lefkoşa, North Cyprus, Turkey

Address correspondence to: Nail Bulakbaşı
E-mail: *nail.bulakbasi@neu.edu.tr*

Objective: The middle interhemispheric (MIH) variant of holoprosencephaly (HPE) is the incomplete separation of midline cerebral hemispheres with the absence of callosal body. We aimed to describe the additional knowledge of diffusion tensor imaging (DTI) over conventional MRI in the evaluation of patients with MIH variant of HPE.
Methods: Conventional MRI and DTI data of five patients were retrospectively evaluated. The parenchymal anomalies as well as changes at white matter tracts were systematically reviewed.
Results: Except the callosal body and central cingulum fibres, which were missing in all patients, all other major white matter tracts (superior and inferior longitudinal, superior and inferior fronto-occipital, subcallosal and uncinate fasciculi and anterior commissure) had a normal course, thickness and integrity on diffusion tensor images. The genial and splenial callosal fibres were altered and rarefied on tractography. All patients had a central ventricular notch extending into the non-cleaved heterotopic grey matter involving the body of the corpus callosum, which is very typical for the MIH variant of HPE. The remnant traversing white matter fibres above the non-cleaved heterotopic grey matter and incomplete partition of the interhemispheric fissure were also identified. No Probst bundles were detected. A single common ventricle without the septum pellucidum was noted in all patients. One patient had incomplete partition of the thalami, and two patients had abnormally oriented thalami without any prominent interthalamic connection. Vertically oriented hippocampi were detected in four out of five patients. Three patients had relatively flat and vertically oriented Sylvian fissures and in two patients, fissures were abnormally connected over the vertex.
Conclusion: Additional DTI findings can not only clearly reveal the white matter alterations better than conventional MRI but also provide a better understanding of the aetiological changes that cause the MIH variant of HPE.
Advances in knowledge: DTI can provide a better analysis of cerebral white matter connectivity and promotes understanding of the underlying microstructural changes that occur in patients with the MIH variant of HPE.

INTRODUCTION

DeMyer et al[1,2] classified holoprosencephaly (HPE) into three major subtypes, alobar, semi-lobar and lobar, according to the severity of the congenital malformations and clinical findings. The middle interhemispheric (MIH) variant of HPE or syntelencephaly was originally described as a type of semi-lobar HPE[3] but was then classified as a different and distinct cliniconeuroradiologic subtype of HPE.[4,5] The MIH variant has similar incidence when compared with other HPE variants.[3,6] By definition, it is an abnormal midline connection of the cerebral hemispheres in the posterior frontal and the anterior parietal regions, with normal interhemispheric separation of the basal forebrain, anterior frontal lobes and occipital regions.[3,4] Typically, the genu and splenium of the corpus callosum are formed, but the body is absent.[3–5,7]

High-resolution conventional MRI can usually reveal sufficient anatomic information about cerebral parenchyma, but diffusion tensor imaging (DTI) can provide more detailed information, which cannot be obtained by conventional MRI, about the visualization and connectivity of white matter structures and anomalies.[8–13] In this article, we aimed to describe the additional knowledge of DTI over conventional MRI obtained by using a 3-T MRI scanner in five patients with MIH variant of HPE and discuss our findings with previously published data.

METHODS AND MATERIALS

Patient population

The MRI and DTI data of five patients (three males and two females) with MRI features of the MIH variant of HPE were retrospectively evaluated. The mean age of the patients was 2.8 ± 1.6 years, ranging from 13 months to

5 years old. The study was approved by the local review board. Written informed consents were obtained from all legal guardians of patients for MRI examinations and for the review of patient records and images.

MRI parameters

Images were acquired using a 3-T MRI scanner (Achieva, Philips Medical Systems, Best, Netherlands) equipped with explorer gradients (40 mT m^{-1}) by using a eight-element arrayed radio frequency head coil, with the eight-channel receiver system.

In each patient, axial inversion-recovery T_1 weighted images (T1WIs) [repetition time (TR)/echo time (TE)/inversion time 2000/20/800 ms and echo train length (ETL) 7] with 512 × 400 matrix size, turbo field echo T_2 weighted images (TR/TE 3000/80 ms and ETL 15) with 436 × 640 matrix size and fluid-attenuated inversion-recovery images (TR/TE/inversion time 11000/125/2800 ms and ETL 27) with 432 × 384 matrix size were obtained by using 4.5-mm slice thickness and 220-mm field of view (FOV). Sagittal high-resolution three-dimensional (3D) turbo field echo T1WIs (shortest TR/TE, ETL 240) were also acquired by using 1-mm slice thickness, 220-mm FOV and 252 × 288 matrix size.

The DTI sequence was obtained by single-shot spin-echo echoplanar imaging (user-defined and shortest TR/TE and ETL 59) with diffusion gradients applied in 16 non-collinear directions including $b = 0$ with $b = 800$ s mm^{-2} value and with 224 × 224-mm FOV, 128 × 112-mm acquisition matrix and 2-mm slice thickness. 60 axial slices were acquired, parallel to the anteroposterior commissure line. All images were zero filled to the final reconstruction matrix of 256 × 256 and to the reconstructed voxel size of 1.75/1.75/2 mm. Two data sets were acquired with a reduction factor of 2 to improve the signal-to-noise ratio, leading to a total acquisition time of 5 min.

DTI data were analyzed on the Philips expanded workstation with release 2.5.3.0. by using the FiberTrak package. 3D T1WIs were used as background images for DTI data evaluation. Colour-coded fractional anisotropy (FA) maps were acquired. For fibre tracking, 3D reconstructions were made by using an algorithm based on fibre assignment by continuous tracking method[8] using a minimum FA value of 0.15, maximum angle change of 35° and minimum fibre length of 10 mm. A DTI atlas was used to guide the placement of two or more seed points and the assessment of white matter bundles.[14]

Patient evaluation

Two investigators (NB and MK) evaluated the MRI and DTI data of all patients by consensus. The presence, shape and location of the following anatomic structures were systematically evaluated: the Sylvian fissure, cingulate and callosal sulci and gyri, fornix, hippocampus and parahippocampal gyrus, septum pellucidum, optic tracts, hypothalamus and pituitary gland, olfactory sulcus and bulb. The presence and location of the heterotopic grey matter, the shape and dimension of the ventricular system and the coexistence of vascular or any other parenchymal anomalies were also noted. The caudate and lentiform nuclei, thalami and their orientation were graded according to previously published data.[15] The integrity, course and abnormalities of superior and inferior longitudinal, superior and inferior fronto-occipital, subcallosal and uncinate fasciculi, anterior commissure, cingulum and corpus callosum were evaluated on FA maps. The corticospinal tracts and cerebellar peduncles were also assessed by DTI. The 3D reconstruction of the corpus callosum fibres was obtained by using the tractography algorithm.

RESULTS

All patients were referred to neuroimaging because of developmental delay, microcephaly and/or accompanying mild-to-moderate different motor anomalies. They have never had any epileptic seizures. None of the patients had a dorsal cyst, hydrocephalus or dysmorphic craniofacial anomalies. In all patients, the inner and middle ear structures, the olfactory sulci and bulb and the optic chiasm were evaluated as normal on MR images. The abnormal conventional MRI findings of the patients are summarized in Table 1 and are shown in Figures 1–3.

A central ventricular notch extending into the unseparated white matter between the thickened dysplastic cortices was noted in all patients (Figure 1a). This ventricular notch was a very typical finding for the MIH variant of HPE.

The major white matter tracts including the superior and inferior longitudinal, superior and inferior fronto-occipital, subcallosal and uncinate fasciculi and anterior commissure had a normal course, thickness and integrity, except the corpus callosum and cingulum on diffusion tensor images. No cingulum bundles were identified at the level of the fused hemispheres in any of the patients. None of the cases had a normal and complete corpus callosum (Figure 1). DTI has confirmed not only the absence of the callosal body fibres, but also the presence of genial and splenial fibres of the corpus callosum normally running into the other hemisphere; but, they have already altered and rarefied on tractography maps (Figure 1b). A transhemispheric unseparated white matter between the thickened dysplastic cortices was identified in all patients, instead of the callosal body just above the ventricular notch (Figures 1 and 3). This remnant thick white matter bundle traversing from one hemisphere to another was coded as red on diffusion tensor images (Figures 1 and 3). No Probst bundles were detected on diffusion tensor images. Temporal lobes were well formed with complete separation of the inferior fronto-occipital fasciculi. The anterior commissure was fully developed in all patients. All our patients had normal corticospinal tracts and normal cerebellar peduncles at the level of the medulla oblongata. No additional brain stem or cerebellar anomaly was noted.

Ethical standards and patient consent

We declare that all human and animal studies have been approved by the Near East University Ethics Committee and have therefore been performed in accordance with the ethical standards laid down in the 1964 Declaration of Helsinki and its later amendments. We declare that all patients gave informed consent prior to inclusion in this study.

DISCUSSION

HPE is the result of impaired cleavage of the forebrain; but, in fact, it is a more complex malformation involving not only the

Table 1. Abnormal MRI findings

Parameters	Patient 1	Patient 2	Patient 3	Patient 4	Patient 5
Age/sex	15 months/female	14 months/male	13 months/male	5 years/male	18 months/female
Sylvian fissure	Flat and vertically oriented Abnormally connected	Normal	Flat and vertically oriented Abnormally connected Abnormal gyral segmentation with extraordinary sulci	Normal	Flat and vertically oriented
Interhemispheric fissure	Incomplete partition	Incomplete partition	Incomplete partition	Incomplete partition	Incomplete partition
Cingulate gyrus and sulcus	Partially absent	Partially absent	Absent	Absent	Partially absent
Dysplastic cortex	Frontal and parietal	R occipital	Frontal and R perisylvian	Frontal	Frontal and R parietal
Corpus callosum	Partially absent genu and splenium Completely absent body	Normal genu Partially absent body Normal splenium	Partially absent genu and splenium Completely absent body	Normal genu Completely absent body Normal splenium	Normal genu Completely absent body Normal splenium
Thalami	Abnormally oriented No massa	Normal	Abnormally oriented No massa	Normal	Incomplete partition
Septum pellucidum	Absent	Absent	Absent	Absent	Absent
Third ventricle	Dilated	Normal	Dilated	Dilated	Dilated
Lateral ventricle	Atrial dilatation vertical orientation	Normal	Atrial dilatation vertical orientation	Atrial dilatation vertical orientation	Atrial dilatation vertical orientation
Parahippocampal gyrus	Hypoplastic	R hypoplastic	Hypoplastic	Hypoplastic	Hypoplastic
Hippocampal orientation	Abnormal	Normal	Abnormal	Abnormal	Abnormal
Collateral sulcus orientation	Deep and vertical	Normal	Deep and vertical	Deep and vertical	Deep and vertical
Vascular anomaly	Azygos ACA	Normal	Azygos ACA	Normal	Azygos ACA
Additional findings	–	Ectopic neurohypophysis and hypoplastic stalk	R dysplastic lentiform nucleus Atretic frontal cephalocele	–	–

ACA, anterior cerebral artery; R, right.

forebrain but also the whole brain, eyes, skull, nose, teeth, lip, palate and cerebral vascularization.[6,7,16] HPE has a range of forebrain malformations with a decreasing severity from the alobar to semi-lobar to lobar forms without any clear-cut distinction among the different subcategories.[16] In the alobar HPE, the cerebral hemispheres as well as the basal ganglia, thalami and hypothalami are completely unseparated, resulting in a single midline forebrain monoventricle, which often communicates with a dorsal cyst, and the interhemispheric fissure, falx cerebri and corpus callosum are absent.[6,16] In the semi-lobar HPE, the anterior hemispheres (mainly the frontal lobes) and the basal ganglia, thalami and hypothalami are partly separated, but the posterior hemispheres, the posterior horns and trigones of the lateral ventricles, the splenium of the corpus callosum, the posterior parts of the interhemispheric fissure and the falx cerebri are completely formed.[6,16] In the lobar HPE, the lack of separation is present in the basal frontal lobes as well as in the basal ganglia, thalami and hypothalami in a less variable degree; so, the anterior horns of the lateral ventricles, the genu and the rostrum of the corpus callosum, the anterior parts of the interhemispheric fissure and the falx cerebri are hypoplastic.[6,16]

In terms of severity, the MIH variant is somewhere between the semi-lobar and lobar forms, closer to the lobar than alobar form, according to functional measures.[3–5,17] Contrary to the severe impairment in the early embryonic development causing the classical HPE forms, such as insufficient ventralization or excessive dorsalization of the forebrain,[3,4] a less severe impairment such as a defect of dorsal–ventral induction of the telencephalon and more specifically a lack of induction of the dorsal

Figure 1. Patient 1 (15-month-old female): the sagittal three-dimensional (3D) turbo field echo (TFE) T_1 weighted image (T1WI) (a) through the midline revealing the genu (asterisk) and the splenium (triangle) of the corpus callosum. The callosal body is absent in the region of non-cleaved parenchyma. There is a ventricular notch (white arrow) towards the white matter (black arrow) between the dysplastic cortices. 3D tractography of the same patient at the same mid-sagittal plane (b) showing the altered and rarefied genial (white arrowheads) and splenial fibres (concave white arrowheads), as well as the absence of callosal body fibres. Also, note the transhemispheric fibres (white arrow) above the non-cleaved white matter between the thickened dysplastic cortices. An axial 3D TFE T1WI (c) showing the bilateral vertically oriented Sylvian fissures with a thickened dysplastic cortex (black arrows). Note the unseparated white matter (short white arrows) between the thickened dysplastic cortices in both the T1WI (c) and fractional anisotropy (FA) map (d). The superior longitudinal fasciculus (white arrowheads), subcallosal fasciculus (long white arrows) and the fibres of the corona radiata (yellow arrows) are showing a normal course, thickness and integrity on the FA map (d). Also, note the transhemispheric orientation of white matter tracts (short white arrows), which is coded as red. For colour image see online.

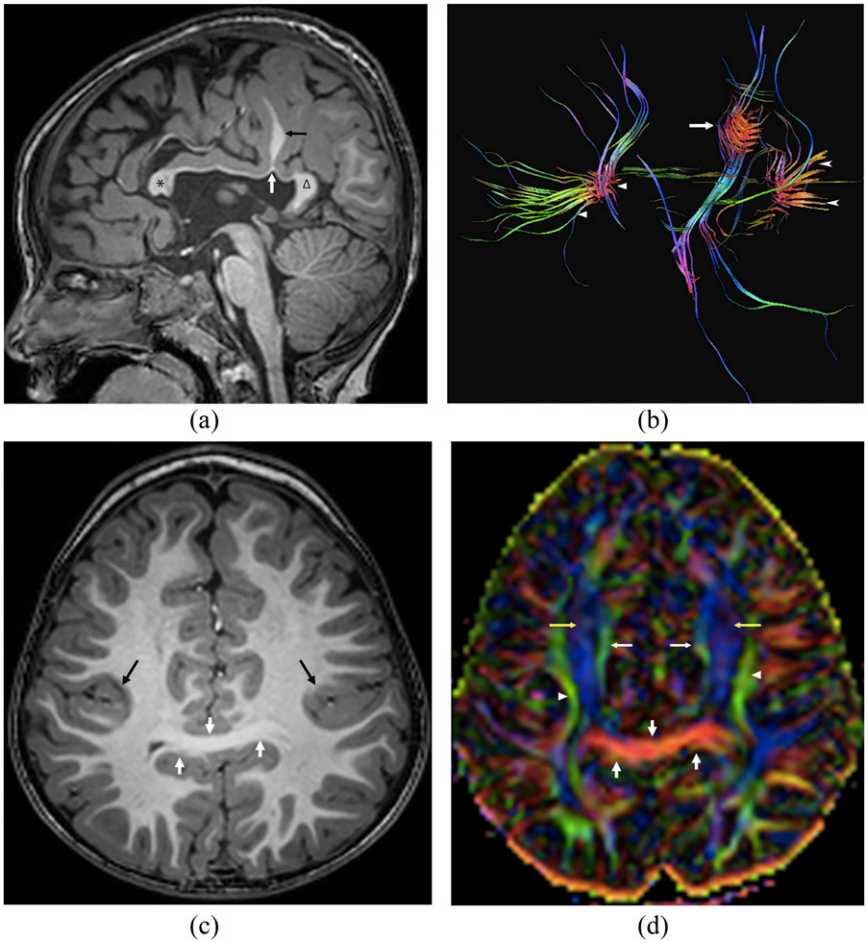

midline structures is usually the cause of the MIH variant of HPE.[5,16] By means of this partial lack of dorsal–ventral induction, the impaired cleavage of cerebral hemispheres is more posteriorly located in the MIH variant (posterior frontal and parietal lobes) than in other classical HPE forms, in which the lack of separation is dedicated to the anterior hemispheres, *i.e.* mainly to the frontal lobes in variable degrees. Owing to the more posterior location of this cortical incomplete separation in the MIH variant, the other associated structural anomalies are also more posteriorly (*i.e.* centrally) located than other HPE forms such as the lack of the middle part of the interhemispheric fissure and falx cerebri, the isolated absence of the callosal body, the absence of the septum pellucidum causing a common telencephalic ventricle and the centrally located midline supraventricular heterotopic grey matter or dysplastic cortex.[3,4,6,7,16,17]

Contrary to the normal embryogenesis of the corpus callosum in the anteroposterior direction, the MIH variant of HPE is the only brain anomaly in which the posterior corpus callosum forms in the absence of anterior or middle callosal formation.[16] This is a very pathognomonic finding for the MIH variant and helps in differentiating it from other HPE forms. Besides the body of the corpus callosum, other centrally located structures such as the cingulum fibres, the cingulate cortex and sulci and thalami are more frequently affected than the more peripheral structures such as the globus pallidi or lentiform nuclei. As previously reported in the literature, the thalami were not separated in one-third of cases with the MIH variant of HPE.[6,16] We detected unseparated thalamus in only one case; but, in the four out of five cases, the thalami were fully separated. In addition, in two out of these four cases, there was an

Figure 2. Patient 3 (13-month-old male): an axial three-dimensional (3D) turbo field echo (TFE) T_1 weighted image (T1WI) (a) revealing the incomplete separation of the white matter (black arrow) and abnormal sulcation (white arrows). An axial 3D TFE T1WI (b) of the same patient passing through the basal ganglia level showing bilateral flat Sylvian fissures with perisylvian cortical dysplasia (black arrows) involving the right lentiform nucleus. Also, note the frontal continuum of the dysplastic cortex (white arrowheads) and the right frontal atretic cephalocele (white arrow). The coronal 3D TFE T1WI (c) showing a widely separated thalamus (black asterisks) without a prominent interthalamic connection and also the vertically oriented deep collateral sulci (white arrows) and dysplastic cortex (black arrowhead) with incomplete separation of the interhemispheric fissure (white arrowhead). Also, note the common occipital ventricle (white asterisk) without any identifiable septum pellucidum and flat Sylvian fissures with a right perisylvian cortical dysplasia (black arrow).

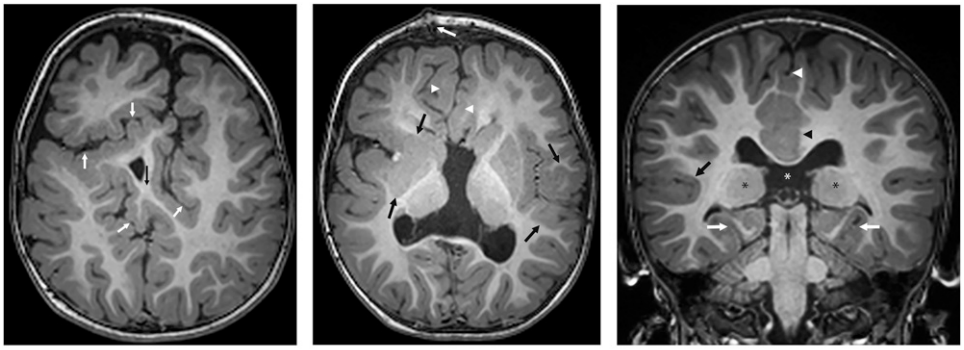

(a) (b) (c)

abnormal vertical orientation and overseparation of the thalami without any prominent interthalamic connection. Lentiform nucleus involvement in one of our patients was due to the penetration of perisylvian heterotopy into right lentiform nuclei rather than a true induction anomaly. Contrary to other HPE variants, the anterior hemispheric structures are also well formed in the MIH variant. Furthermore, a bunch of neural tube closure defects such as cephalocele, myelomeningocele or Chiari II malformation have been defined in patients with MIH variant of HPE.[7] Similarly, one of our patients had an atretic frontal cephalocele. These findings are the result of the complexity and phenotypic heterogeneity of HPE.

The DTI findings of our cases revealed the normal white matter tracts except the corpus callosum and cingulum fibres. We detected a normal callosal connection between the contralateral frontal and occipital lobes in our cases, but a remarkably reduced diversity in the genial and splenial areas. We could not identify the homotropic or heterotopic fibres owing to the lack of anatomic symmetry in patients with MIH variant of HPE and also owing to insufficient resolution of the DTI data. The normal course and the thickness of the corticospinal tracts and cerebellar peduncles at the level of the medulla oblongata in our patients also helped in differentiating the MIH variant from the more severe HPE forms (alobar and semi-lobar), in which the

Figure 3. Patient 5 (18-month-old female): an axial three-dimensional (3D) turbo field echo (TFE) T_1 weighted image (T1WI) (a) showing bilateral flat and vertically oriented Sylvian fissures (black arrows) and right parietal dysplastic cortex (black arrowhead). The axial 3D TFE T1WI (a) and fractional anisotropy map (b) also showing the dysplastic cortex (white asterisks) with incomplete separation of the interhemispheric fissure and transhemispheric fibres (white arrows) in the non-cleaved white matter between the thickened dysplastic cortices. The coronal 3D TFE T1WI (c) revealing the incomplete separation of the thalami (black arrow), hypoplastic hippocampus (white arrow) and the absence of the septum pellucidum in a unicameral telencephalic third ventricle (asterisk). Also, note the dysplastic continuum of the non-cleaved cortex (black arrowhead) and incomplete formation of the interhemispheric fissure (white arrowhead), as well as the right parietal dysplastic cortex (concave black arrowhead).

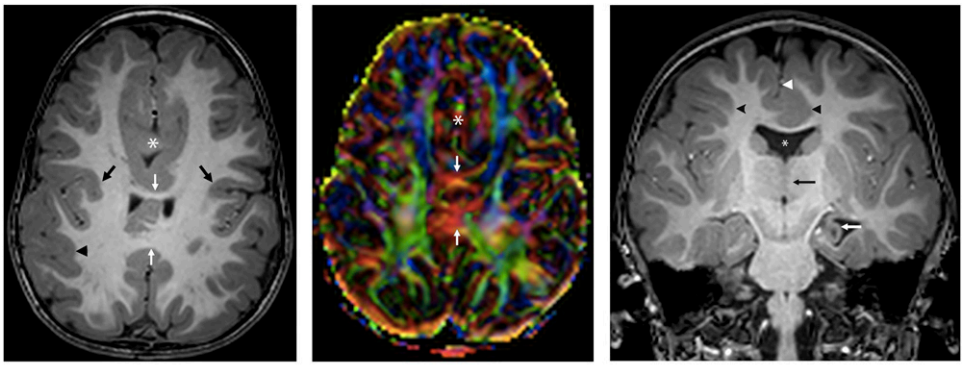

(a) (b) (c)

corticospinal tracts were not identifiable at the level of the medulla oblongata.[9,13] Also, no Probst bundles, which run longitudinally and represent misdirected callosal fibres seen in callosal dysgenesis, were identified in any of our cases. This is also very compatible with the literature because typically, Probst bundles are never observed in HPE, conversely to other isolated or syndromic corpus callosum agenesis.[6,9,13]

We have also observed a transverse thick white matter bundle traversing between the two hemispheres, along the dysplastic cortex located where the body of the corpus callosum was missing, similar to the previously published data.[13] These fibres were interpreted as remnant or dislocated white matter tracts, which probably take over the function of the missing callosal body fibres. In addition, a central ventricular notch extending into the unseparated white matter between the thickened dysplastic cortices, which has also been noted in all patients, is very typical for the MIH variant of HPE and is not seen in any of the other HPE subtypes.

In our patients, we identified well-differentiated temporal lobes, vertically oriented hippocampi and the normal course of inferior fronto-occipital and inferior longitudinal fasciculi. Fully developed temporal lobes with well-separated inferior fronto-occipital fasciculi also help in differentiating the MIH variant form of semi-lobar HPE.[11,13] Furthermore, Rollins[11] reported bilateral fusion of both inferior fronto-occipital fasciculi, the absence of demarcation between the inferior and superior longitudinal fasciculi and thickened and dysplastic fornices in patients with semi-lobar HPE, contrary to the normal appearance of these structures in patients with the MIH variant.

There were several certain limitations in this study. First, the data of the patient population are too small for statistics. The MIH variant of HPE is quite rare to allow collection of enough data. Furthermore, we had to evaluate the patients in consensus because of the huge diversity of DTI findings in a small patient group. Second, DTI data were acquired by using routine protocol with 16 diffusion directions in a 3-T scanner in this study, but DTI metrics obtained by higher directions and more advanced techniques such as high angular resolution diffusion-weighted imaging[18] or q-ball imaging[19] can provide a more precise evaluation of white matter tracts.[12] Third, we used a commercially available post-processing package supplied by the vendor. Discussing the pros and cons of this software or comparing it with other homemade or commercial ones is out of the scope of this study, but we believed that the usage of more sophisticated post-processing techniques can improve the image quality of DTI data, allowing a more precise evaluation of the fibre anatomy. Besides its technical properties, the low reproducibility of fibre tractography should be considered in the evaluation of these patients, because it may affect the interpretation results.[13] The limitations of tractography are mostly derived from the discrepancies between the following parameters: the scale of the axonal diameter, the imaging voxel size (low spatial resolution), the noise contained in DTI data and image artefacts.[20] Also, different acquisition parameters, scanner types and magnetic field strength may also affect tractography performance. The poor performance of tractography in crossing fibres is also a well-known problem and can cause incomplete tracking in the regions of multiple populations of white matter tracts and may result in spurious fibres. Although there are some certain protocols to increase the reproducibility of DTI tractography,[21] it is quite difficult to apply these protocols in brain malformations owing to abnormal brain anatomy.[13]

CONCLUSION

DTI can provide additional knowledge over conventional MRI by showing the white matter abnormalities more precisely than conventional MRI in patients with MIH variant of HPE. DTI can provide a better analysis of cerebral connectivity and promotes understanding of the underlying microstructural changes that occur in patients with HPE and its variants. Especially, the prenatal applications of advanced DTI techniques will clear up the basic mechanisms of axonal guidance and white matter connectivity within the developing brain. Further investigations are needed to collect more sufficient DTI data, which clarify the exact role of DTI as well as the potential embryogenetic mechanisms in patients with MIH variant of HPE.

REFERENCES

1. DeMyer W, Zeman W. Alobar holoprosencephaly (arhinencephaly) with median cleft lip and palate: clinical, electroencephalographic and nosologic considerations. *Confin Neurol* 1963; **23**: 1–36.
2. DeMyer W, Zeman W, Palmer CG. The face predicts the brain: diagnostic significance of median facial anomalies for holoprosencephaly (arhinencephaly). *Pediatrics* 1964; **34**: 256–63.
3. Barkovich AJ, Quint DJ. Middle interhemispheric fusion: an unusual variant of holoprosencephaly. *AJNR Am J Neuroradiol* 1993; **14**: 431–40.
4. Simon EM, Barkovich AJ. Holoprosencephaly: new concepts. *Magn Reson Imaging Clin N Am* 2001; **9**: 149–64, viii–ix.
5. Lewis AJ, Simon EM, Barkovich AJ, Clegg NJ, Delgado MR, Levey E, et al. Middle interhemispheric variant of holoprosencephaly: a distinct cliniconeuroradiologic subtype. *Neurology* 2002; **59**: 1860–5. doi: http://dx.doi.org/10.1212/01.WNL.0000037483.31989.B9
6. Hahn JS, Barnes PD. Neuroimaging advances in holoprosencephaly: refining the spectrum of the midline malformation. *Am J Med Genet C Semin Med Genet* 2010; **154C**: 120–32. doi: http://dx.doi.org/10.1002/ajmg.c.30238
7. Simon EM, Hevner RF, Pinter JD, Clegg NJ, Delgado M, Kinsman SL, et al. The middle interhemispheric variant of holoprosencephaly. *AJNR Am J Neuroradiol* 2002; **23**: 151–6. Erratum in: *AJNR Am J Neuroradiol* 2002; **23**: 742.
8. Mori S, Crain BJ, Chacko VP, van Zijl PC. Three-dimensional tracking of axonal projections in the brain by magnetic resonance imaging. *Ann Neurol* 1999; **45**: 265–9. doi: http://dx.doi.org/10.1002/1531-8249(199902)45:2<265::AID-ANA21>3.0.CO;2-3

9. Albayram S, Melhem ER, Mori S, Zinreich SJ, Barkovich AJ, Kinsman SL. Holoprosencephaly in children: diffusion tensor MR imaging of white matter tracts of the brainstem—initial experience. *Radiology* 2002; **223**: 645–51. doi: http://dx.doi.org/10.1148/radiol.2233011197
10. Kinsman SL. White matter imaging in holoprosencephaly in children. *Curr Opin Neurol* 2004; **17**: 115–9. doi: http://dx.doi.org/10.1097/00019052-200404000-00006
11. Rollins N. Semilobar holoprosencephaly seen with diffusion tensor imaging and fiber tracking. *AJNR Am J Neuroradiol* 2005; **26**: 2148–52.
12. Wahl M, Barkovich AJ, Mukherjee P. Diffusion imaging and tractography of congenital brain malformations. *Pediatr Radiol* 2010; **40**: 59–67. doi: http://dx.doi.org/10.1007/s00247-009-1448-6
13. Verschuuren S, Poretti A, Meoded A, Izbudak I, Huisman TAGM. Diffusion tensor imaging and fiber tractography in syntelencephaly. *Neurographics* 2013; **3**: 164–8. doi: http://dx.doi.org/10.3174/ng.4130066
14. Cho ZH, Calamente F, Chi JG, eds. *7.0 Tesla MRI brain white matter atlas*. Berlin, Heidelberg: Springer & Verlag; 2015.
15. Simon EM, Hevner R, Pinter JD, Clegg NJ, Miller VS, Kinsman SL, et al. Assessment of the deep gray nuclei in holoprosencephaly. *AJNR Am J Neuroradiol* 2000; **21**: 1955–61.
16. Marcorelles P, Laquerriere A. Neuropathology of holoprosencephaly. *Am J Med Genet C Semin Med Genet* 2010; **154C**: 109–19. doi: http://dx.doi.org/10.1002/ajmg.c.30249
17. Winter TC, Kennedy AM, Woodward PJ. Holoprosencephaly: a survey of the entity, with embryology and fetal imaging. *Radiographics* 2015; **35**: 275–90. doi: http://dx.doi.org/10.1148/rg.351140040
18. Ozarslan E, Mareci TH. Generalized diffusion tensor imaging and analytical relationships between diffusion tensor imaging and high angular resolution diffusion imaging. *Magn Reson Med* 2003; **50**: 955–65.
19. Tuch DS. Q-ball imaging. *Magn Reson Med* 2004; **52**: 1358–72. doi: http://dx.doi.org/10.1002/mrm.20279
20. Ciccarelli O, Catani M, Johansen-Berg H, Clark C, Thompson A. Diffusion-based tractography in neurological disorders: concepts, applications, and future developments. *Lancet Neurol* 2008; **7**: 715–27. doi: http://dx.doi.org/10.1016/S1474-4422(08)70163-7
21. Wakana S, Caprihan A, Panzenboeck MM, Fallon JH, Perry M, Gollub RL, et al. Reproducibility of quantitative tractography methods applied to cerebral white matter. *Neuroimage* 2007; **36**: 630–44. doi: http://dx.doi.org/10.1016/j.neuroimage.2007.02.049